Liao et al. *Zool. Res.* 2026, 47(3): 785−797
https://doi.org/10.24272/j.issn.2095-8137.2025.492
https://cstr.cn/32248.14.zr.2025.492

ZR | Zoological Research

Article Open Access

Functional characterization of HR-CATH2, a novel cathelicidin from *Hoplobatrachus rugulosus* with anti-sepsis activity

Hang Liao[1,#], Shian Lai[2,#], Kai Wang[3,#], Jinwei Chai[1,3], Weiyong Zeng[3], Jinqiao Li[1], Jiena Wu[1], Yongtao Luo[1], Lixia Shu[1], Xin Chen[3], Yuxin Gong[3], Xueqing Xu[1,*]

[1] *NMPA Key Laboratory for Research and Evaluation of Drug Metabolism*, *Guangdong Provincial Key Laboratory of New Drug Screening*, *School of Pharmaceutical Sciences*, *Southern Medical University*, *Guangzhou*, *Guangdong* 510515, *China*

[2] *Department of Life Sciences*, *Graduate School of Arts and Sciences*, *The University of Tokyo*, *3-8-1 Komaba*, *Meguro*, *Tokyo* 153-8902, *Japan*

[3] *Department of Pulmonary and Critical Care Medicine*, *Zhujiang Hospital*, *Southern Medical University*, *Guangzhou*, *Guangdong* 510280, *China*

ABSTRACT

Cathelicidins are central effectors of innate host immunity against invading microorganisms and represent a promising source of next-generation anti-infective agents. However, current understanding of both antimicrobial activity and immunomodulatory function within this peptide family remains incomplete. In the present study, a novel cathelicidin peptide, designated HR-CATH2, was identified from the skin of the Chinese tiger frog (*Hoplobatrachus rugulosus*). The peptide consisted of 30 amino acid residues (GRCNLLCKAKKKLRAVGNKIKEIKNVVFNR) and adopted a highly amphipathic α-helical structure. Functional analyses indicated that HR-CATH2 exerted potent antimicrobial activity through induction of intracellular reactive oxygen species (ROS) accumulation and direct disruption of bacterial membrane integrity. Moreover, HR-CATH2 inhibited overproduction of proinflammatory cytokines (interleukin-6, interleukin-1β, and tumor necrosis factor-α) and nitric oxide (NO) in RAW264.7 cells through lipopolysaccharide (LPS) binding and consequent inactivation of MAPK signaling. *In vivo*, HR-CATH2 markedly attenuated the acute inflammatory response and reduced mortality in mice subjected to cecal ligation and puncture (CLP)-induced sepsis. Together, these findings identify HR-CATH2 as a multifunctional cathelicidin with antibacterial, LPS-neutralizing, and anti-inflammatory activities, and support its potential as a therapeutic candidate for bacterial infectious diseases, including sepsis.

Keywords: Antimicrobial peptide; Cathelicidin; Sepsis; Macrophage; frog; *Hoplobatrachus rugulosus*

INTRODUCTION

Sepsis, defined as a dysregulated host response to infection, remains a leading cause of mortality in intensive care units worldwide (Cecconi et al., 2018). Current clinical management relies primarily on fluid resuscitation and intravenous antimicrobial therapy (Liu et al., 2017; Rhodes et al., 2017). Corticosteroids can provide short-term therapeutic benefit in selected settings, but long-term use is constrained by substantial adverse effects, including osteoporosis, aseptic joint necrosis, and disorders affecting digestive and cardiovascular systems (Buchman, 2001; Rhodes et al., 2017; Vandewalle et al., 2021). In addition, corticosteroid resistance may further contribute to unfavorable outcomes in sepsis (Vandewalle et al., 2021). Although antimicrobial therapy is indispensable, widespread antibiotic use has accelerated the emergence of resistant microorganisms, thereby increasing medical costs, prolonging hospitalization, and contributing to approximately 700 000 deaths worldwide each year (Curren et al., 2022; Willyard, 2017). Antibiotic-mediated bacterial lysis can also intensify systemic inflammation through release of inflammatory stimuli such as lipopolysaccharide (LPS), subsequently worsening disease severity and, in some cases, contributing to death. These limitations have prompted extensive efforts to identify novel therapeutic candidates for sepsis that combine multiple beneficial activities with minimal adverse effects.

Received: 02 December 2025; Accepted: 28 December 2025; Online: 29 December 2025

Foundation items: This work was supported by the Key Research and Development Program of Guangzhou Science and Technology Plan Project (2024B03J0011), Guangdong Basic and Applied Basic Research Foundation (2024A1515011603), and National Natural Science Foundation of China (32570586, 82504889)

[#]Authors contributed equally to this work

*Corresponding author, E-mail: xu2003@smu.edu.cn

Antimicrobial peptides (AMPs) are integral components of innate immunity and serve as an early defense barrier against invasive pathogens (Lazzaro et al., 2020). Cathelicidins, one of the major AMP families, are commonly derived from precursor proteins containing a highly conserved cathelin domain followed by a mature C-terminal peptide (Zanetti et al., 2002). Many cathelicidins adopt an amphipathic α-helical conformation that promotes membrane permeabilization through oligomeric interactions with phospholipid bilayers, ultimately disrupting bacterial membrane integrity and causing cell death (Bals & Wilson, 2003; Kościuczuk et al., 2012). Beyond direct antimicrobial activity, cathelicidins have been shown to exert potent antitumor, antiviral, antioxidant, LPS-neutralizing (Wei et al., 2013), wound-healing, and anti-inflammatory effects (Wong et al., 2013). This multifunctional profile, together with a relatively low propensity to induce bacterial resistance, has made cathelicidins attractive candidates for adjunctive sepsis therapy (Chai et al., 2021; Ho et al., 2020; Li et al., 2020).

To date, more than 5 000 AMPs have been cataloged in the Antimicrobial Peptide Database (APD6), with amphibians representing one of the richest known sources of these molecules (Xu & Lai, 2015). Nevertheless, despite the vast diversity of amphibian species, structural and functional characterization of amphibian-derived cathelicidins remains limited. *Hoplobatrachus rugulosus*, also known as the Chinese tiger frog, is widely distributed throughout Southeast Asia (Fei et al., 2012) and inhabits moist environments conducive to the proliferation of pathogenic bacteria. Furthermore, *H. rugulosus* has been described in Chinese traditional medical literature as having swelling-reducing and cough-relieving properties (Li et al., 2013a), suggesting the presence of bioactive antimicrobial and anti-inflammatory components in the skin. To date, only HR-CATH (Chen et al., 2021), Cathelicidin-HR (Wiriyaampaiwong et al., 2022), Brevinin-1GHd (Tian et al., 2023), Tigerinin-1R (Pantic et al., 2014), and TK-HR (Wu et al., 2023) have been reported from *H. rugulosus* skin, indicating that additional constituents remain to be identified.

In the present study, a novel cathelicidin sequence encoding HR-CATH2 was identified from the skin transcriptome of *H. rugulosus*. Compared with AMPs previously identified from *Hoplobatrachus* species and with other known cathelicidins, HR-CATH2 displayed only partial similarity to the N-terminal region of cathelicidins such as HR-CATH and retained a basic arginine residue at the C terminus. Secondary-structure prediction further indicated an unusually high helical content, with 26 of 30 residues predicted to participate in α-helix formation, suggesting structural features distinct from those of other *H. rugulosus* AMPs. This unusual structural profile raises the possibility that HR-CATH2 may possess biological activities or molecular targets not observed in previously reported peptides from this species. Functional analyses demonstrated that HR-CATH2 exerted both direct anti-inflammatory effects through targeting macrophage-associated pathways and dual antimicrobial and LPS-neutralizing activities. HR-CATH2 also conferred protection against sepsis in mice. Collectively, these findings indicate that HR-CATH2 is a promising therapeutic candidate for the treatment of bacterial infections and inflammatory diseases such as sepsis.

MATERIALS AND METHODS

Animals and ethical statement

Adult *H. rugulosus* frogs of both sexes weighing 170–230 g (*n*=3) were obtained from a licensed commercial farm in a market in Baiyun District, Guangzhou, China. Although *H. rugulosus* is classified as a National Grade II Protected species, its use in this study complied with all relevant regulations because the species was included in the 2021 “List of Key Protected Aquatic Wildlife under Artificial Breeding”. All procedures adhered to the “3R” principles to minimize animal suffering and reduce the number of specimens used.

BALB/c mice weighing 18–25 g were procured from the Experimental Animal Center of Southern Medical University (Guangdong, China) and maintained under controlled conditions at 25°C, 55% humidity, and a 12 h light/12 h dark cycle with lights on at 07: 00 h. All animal experiments were accomplished in strict accordance with the Chinese Law on the Administration of Laboratory Animals and were approved by the Southern Medical University Animal Care and Use Ethics Committee (Approval No.: SMUL202404026).

Sequence identification and peptide synthesis of HR-CATH2

The HR-CATH2 cDNA sequence was obtained from skin transcriptome data of *H. rugulosus* (GSA: CRA034383). HR-CATH2 (purity>95%) was commercially synthesized by Shanghai Gil Biochemical (China). Molecular weight was determined by matrix-assisted laser desorption ionization time-of-flight mass spectrometry (Voyager-DE-PRO MALDI-TOF, SCIEX, USA). Fluorescein isothiocyanate (FITC)-labeled HR-CATH2 was acquired using a FITC conjugation kit (Sangon company, China).

Antimicrobial assays

Minimum inhibitory concentration (MIC) values of HR-CATH2 were determined using a two-fold dilution technique, as described previously (Zeng et al., 2018). To assess peptide stability, HR-CATH2 was exposed to NaCl at different concentrations (0, 50, 100, 200, and 400 mmol/L) or to different temperatures (4, 25, 37, 50, 70 and 90°C), after which MICs were measured. Bactericidal activity against *Escherichia coli* ATCC 25922 was further evaluated using the spread plate method as per previous research (Zeng et al., 2018). Normal saline and meropenem (MIC=0.015 mol/L) served as negative and positive controls, respectively.

Antimicrobial mechanism identification

The antimicrobial mechanism of HR-CATH2 was investigated using scanning electron microscopy (SEM) and propidium iodide (PI) uptake assays as reported in previous studies (Tian et al., 2021; Xiao et al., 2022). Briefly, *E. coli* ATCC 25922 in the logarithmic phase was collected and incubated with HR-CATH2 (1×, 2×, and 4× MICs), or with phosphate-buffered saline (PBS) as a control, for 45 min at 37°C. Bacterial cells were then harvested and gently rinsed with PBS. For PI uptake analysis, the collected bacteria were stained with PI solution (Keygen Biotech, China) for 10 min at 37°C and analyzed by flow cytometry (Becton Dickinson, USA).

For SEM analysis, washed *E. coli* ATCC 25922 cells were exposed to HR-CATH2 (2× MICs) for 45 min at 37°C, fixed in 2.5% glutaraldehyde, and rinsed with PBS at 4°C. Samples were dehydrated sequentially in graded ethanol solutions for 15 min per step and dried with a critical point dryer. After gold sputter coating, the samples were analyzed using a Phenom ProX SEM (Thermo Fisher Scientific, USA). Approximately 6–8 single-sided images were obtained for each sample.

Reactive oxygen species (ROS) detection

Intracellular ROS levels were measured with the free radical probe DCFH-DA according to the manufacturer's instructions. In brief, *E. coli* ATCC 25922 was incubated with different concentrations of HR-CATH2 under the same conditions described for the PI uptake assay. Samples were incubated with 10 μmol/L of DCFH-DA (Sigma-Aldrich, Germany) in the dark at 37°C for 30 min, washed, resuspended in PBS, and analyzed by flow cytometry (Becton Dickinson, USA). For ROS detection, RAW264.7 cells were seeded in 24-well plates at a density of 1.5×10^5 cells per well and cultured overnight. Cells were then treated with HR-CATH2 at 0, 2.5, 5, 10, and 20 μmol/L for 1 h, followed by stimulation with 100 ng/mL LPS (*E. coli* O_{55}:B_5, L6529, Sigma-Aldrich, Germany). After 6 h at 37°C, cells were washed with PBS, stained with 10 μmol/L DCFH-DA at 37°C for 30 min, and observed using a fluorescent inverted microscope (Axio Observe A1, ZEISS, Germany).

Membrane binding measurement

Membrane binding experiments were performed to evaluate the interaction of FITC-labeled HR-CATH2 with bacterial cells and RAW264.7 cells, as described in previous research (Chai et al., 2024). Briefly, bacteria and RAW264.7 cells at the logarithmic phase were collected, washed, resuspended in PBS, and exposed to different doses of FITC-labeled HR-CATH2 (0, 2.5, 5, 10, and 20 μmol/L) for 30 min. After incubation, unbound peptides were removed by careful washing with PBS and fluorescence intensity was quantified using a FACScan flow cytometer (Becton Dickinson, USA). To determine whether HR-CATH2 entered RAW264.7 cells, cells incubated with 20 μmol/L FITC-labeled HR-CATH2 were washed with PBS and then stained with DiI and DAPI (Beyotime Biotechnology, China). After staining for 20 min at room temperature in the dark, cells were examined under a fluorescence microscope at 400× magnification (BX53, Olympus, Japan). Approximately 5–10 single-plane images were acquired from each randomly selected field.

Determination of nitric oxide (NO) and inflammatory cytokine production

For measurement of tumor necrosis factor-α (TNF-α), interleukin-1β (IL-1β), interleukin-6 (IL-6), and NO at the protein level, cell treatments were identical to those used for mRNA expression analysis except that LPS stimulation was extended to 24 h. Concentrations of these factors in the culture medium were then determined with enzyme-linked immunosorbent assay (ELISA) kits (eBioscience, USA) and Griess reagent (Beyotime Biotechnology, China). To exclude the possibility that anti-inflammatory activity resulted solely from LPS binding, RAW264.7 cells were pretreated with HR-CATH2 at 0, 2.5, 5, 10, or 20 μmol/L for 0.5, 1, or 2 h. HR-CATH2 was then removed completely by washing, followed by the addition of LPS for another 24 h of incubation. IL-6 levels were then measured. As further confirmation, macrophages were exposed to HR-CATH2 at 20 μmol/L for up to 2 h, washed carefully to remove residual HR-CATH2, and incubated with LPS for 24 h. IL-6 levels were then measured. As a control, cells were exposed to LPS for 2 h, washed carefully to remove unbound LPS, and then incubated with HR-CATH2 at 20 μmol/L for 24 h. In the negative control group, cells were treated with sterile PBS alone. Each experiment was performed at least three times.

Isothermal titration calorimetry (ITC)

The MicroCal PEAQ-ITC instrument (Malvern Panalytical, UK) was used to evaluate the thermodynamic interaction between HR-CATH2 and LPS. Briefly, HR-CATH2 and LPS were dissolved in PBS (pH 7.2). HR-CATH2 (1 mmol/L) was injected in 1.5 μL aliquots into a constant-temperature cell containing 250 μL of 50 μmol/L LPS at 25°C. A total of 26 injections were performed. Instrument operation and data processing followed our previously described approach (Chai et al., 2021). The experiment was repeated three times.

Surface plasmon resonance imaging (SPRi) analysis

Real-time analysis of HR-CATH2 binding to LPS was performed using the PlexArray HT A100 system (Plexera LLC, USA) as described previously (Chai et al., 2021). Briefly, HR-CATH2 (2 mmol/L) was dissolved in PBS, sonicated, and spotted repeatedly onto multiple locations on the chip. The chip was then incubated in a humid chamber at 4°C for 12 h, washed gently three times with PBS, blocked using 1 mol/L ethanolamine buffer (pH 8.5) for 30 min, and mounted on the device. Instrument operation and data processing were conducted following previous research (Chai et al., 2021).

RNA sequencing (RNA-seq) and transcriptomic analyses

RAW264.7 macrophages were seeded in 35-mm culture dishes and cultured overnight before incubation with 20 μmol/L HR-CATH2 for 4 h. Cells were then collected by centrifugation, and mRNA libraries were constructed from total RNA and sequenced by AZENTA Life Sciences (USA) according to previously described protocols (Wang et al., 2013; Ye et al., 2024). Quality control was performed with Cutadapt v.1.9.1 and RSeQC to generate high-quality clean data (Martin, 2011; Wang et al., 2012). Gene expression levels were quantified as transcripts per million (TPM). Genomic sequences of related species and corresponding gene annotation files were retrieved from multiple genomic databases, including UCSC, NCBI, and Ensembl. Alignment, annotation, expression quantification, differential gene expression analysis, Gene Ontology (GO) enrichment analysis, and Kyoto Encyclopedia of Genes and Genomes (KEGG) enrichment analysis were completed by the sequencing company using HISAT2 v.2.2.1, rMATS v.4.1.0, SAMtools v.0.1.19, ANNOVAR v.2013.02.11, HTSeq v.0.6.1, DESeq2 v.1.26.0, GOSeq v.1.34.1, and KEGG databases (Anders & Huber, 2010; Anders et al., 2015; Kanehisa et al., 2017; Kim et al., 2019; Li et al., 2009; Shen et al., 2014; Wang et al., 2010; Young et al., 2010), respectively.

Western blot analysis

RAW264.7 macrophages were seeded in 6-well plates at a density of 1.0×10^6 cells per well and cultured overnight. Subsequently, cells were pretreated with HR-CATH2 at 0, 2.5, 5, or 10 μmol/L for 1 h, followed by stimulation with 100 ng/mL LPS for another 30 min. Cytoplasmic protein extracts were prepared and analyzed by western blotting according to previously established methods (Tian et al., 2021). Primary antibodies against phospho-JNK/JNK (#4671S; #9252S), phospho-ERK/ERK (#4376S; #4695S), phospho-p38/p38 (#9211S; #9212S), and GAPDH (#5174S) were used at a 1:1 500 dilution. Horseradish peroxidase (HRP)-conjugated secondary antibody (#4414S) was used at a 1:2 000 dilution. All antibodies were obtained from Cell Signaling Technology (USA). The experiment was performed three times.

Effects of HR-CATH2 on cecal ligation and puncture (CLP)-induced septic mice

Sepsis was induced in BALB/c mice using the CLP method, as

described previously (Chai et al., 2021). In short, eight-week-old male BALB/c mice weighing 18–25 g were randomly assigned to four groups (*n*=10 per group): sham-operated group, CLP model group, CLP+dexamethasone (DXM) treatment group, and CLP+HR-CATH2 treatment group. After a 3-day acclimatization period, mice were anesthetized using a mixture of 8 mg/kg xylazine and 100 mg/kg ketamine. The CLP operation was then carried out under aseptic conditions. Septic mice received an intraperitoneal injection of HR-CATH2 (5 mg/kg), DXM (10 mg/kg), or 0.9% sterile saline (sham group) within 1 h post-surgery. Mice were then returned to their cages and observed for 72 h. In subsequent experiments, a separate cohort of mice was treated under the same conditions, with blood, liver, lungs, and kidneys collected at 12 h post-surgery for histopathological analysis, pathological scoring, and inflammatory cytokine determination. Clinical scoring was performed at 24 h, as described previously (Dawulieti et al., 2020). Mice in the sham group underwent the same surgical procedures as those in other groups except that CLP was not performed.

Statistical analysis

All data are presented as mean±standard deviation (SD). Comparisons between two groups were performed with the independent sample *t*-test, while comparisons involving more than two groups were carried out using one-way analysis of variance (ANOVA) followed by Tukey's multiple comparisons test. Survival differences between groups were assessed with the log-rank test. Statistical analyses were performed with GraphPad Prism v.9.0 (GraphPad Software, Inc, USA). $P<0.05$ was considered statistically significant.

RESULTS

Characterization and structural determination of HR-CATH2

The cDNA sequence of the HR-CATH2 precursor was 605 bp in length and was predicted to encode a 153-amino-acid protein. This precursor displayed the characteristic structural organization of cathelicidins, including a 20-residue signal peptide, a 103-residue cathelin domain, and a mature peptide with the sequence GRCNLLCKAKKKLRAVGNKIKEIKNVV FNR. Although the mature peptide exhibited very low homology to other cathelicidins and contained a basic arginine residue at the C-terminus, a feature not previously reported among identified cathelicidins, the N-terminal region shared the highest sequence similarity (76%) with HR-CATH (Figure 1A; Supplementary Figure S1). Based on these characteristics, the mature peptide was designated HR-CATH2. Multi-sequence alignment of HR-CATH2 with cathelicidin precursors from nine frog species further showed that HR-CATH2 retained two highly conserved cysteine residues shared with other frog-derived cathelicidins, whereas lysine and arginine residues were concentrated predominantly at the N-terminal region of most mature cathelicidin peptides (Supplementary Figure S1). The theoretical isoelectric point (pI) and net charge of HR-CATH2 were predicted to be 10.72 and +9, respectively. The calculated molecular mass was 3 442.24 Da, which was highly consistent with the mass spectrometry results obtained for the oxidized form containing an intramolecular disulfide bond (Figure 1B, C).

Secondary-structure prediction by PEP-FOLD3 and SOPMA indicated that HR-CATH2 adopted a predominantly α-helical conformation (Figure 1D, E), with 26 of the 30 residues predicted to participate in helix formation. This proportion represented the highest helical content among cathelicidins with reported secondary structures. Helical wheel projection of residues Asn-4 to Phe-28 showed amphipathic organization, with hydrophobic residues (gray and yellow) and hydrophilic residues (blue, pink, and red) segregated to opposite faces of the helix (Figure 1F). Circular dichroism (CD) spectroscopy further showed that HR-CATH2 in aqueous solution exhibited two negative absorption peaks at 200 and 211 nm, consistent with a predominantly random-coil conformation (Figure 1G). In contrast, CD spectra obtained in SDS/H_2O solutions (30–120 mmol/L) displayed a prominent positive peak at 192 nm and two weak negative peaks at 208 and 222 nm, indicating formation of an α-helical structure. In addition, CD spectra of HR-CATH2 recorded at different temperatures were nearly identical, indicating marked thermal stability of the secondary structure (Figure 1H). When HR-CATH2 was dissolved in SDS solution containing NaCl (0, 100, 200, and 400 mmol/L), the positive peak at 192 nm slowly declined and additional spectral changes appeared (Figure 1I). However, the α-helical content remained unchanged.

Antimicrobial activity and mechanism of HR-CATH2

HR-CATH2 exhibited broad-spectrum antimicrobial activity, with a MIC of 1.5625 μmol/L against the most susceptible microorganism, *Bacillus subtilis* CMCC 63501 (Supplementary Table S1). Notably, antimicrobial activity against *E. coli* ATCC 25922 remained largely unaffected by changes in temperature or salt concentration (Supplementary Figure S2A, B). To distinguish bacteriostatic from bactericidal activity, a time-kill assay was performed. As shown in Supplementary Figure S2C, colony-forming unit (CFU) counts declined sharply with increasing HR-CATH2 concentration and longer incubation time. At 25 μmol/L, HR-CATH2 completely eliminated *E. coli* ATCC 25922 within 90 min, indicating a bactericidal mode of action. In addition, although antimicrobial efficacy remained lower than that of meropenem, the latter did not completely eradicate *E. coli* ATCC 25922 within 180 min under the same conditions.

Binding of FITC-labeled HR-CATH2 to bacterial cells was evaluated by flow cytometry.

As shown in Figure 2A, fluorescence intensity increased in a concentration-dependent manner after exposure to FITC-labeled HR-CATH2, and a significant increase was evident after 15 min of incubation compared with untreated bacteria. Furthermore, PI uptake also increased progressively with increasing HR-CATH2 concentration, indicating concentration-dependent disruption of bacterial membrane integrity (Figure 2B). Consistently, HR-CATH2 induced a concentration-dependent increase in intracellular ROS levels in bacteria (Figure 2C). These findings were further supported by SEM analysis. Untreated *E. coli* ATCC 25922 displayed a regular morphology and a smooth outer membrane (Figure 2D, panel a), whereas HR-CATH2-treated cells exhibited marked ultrastructural damage, including distinct pore formation and cytoplasmic membrane protrusions (Figure 2D, panel b). Collectively, these results suggest that HR-CATH2 initially associates with the negatively charged bacterial membrane and subsequently exerts antimicrobial activity through membrane disruption.

Hemolytic activity and cytotoxicity of HR-CATH2

Assessment of hemolytic activity in mouse erythrocytes showed that HR-CATH2 produced no detectable hemolysis at concentrations up to 40 μmol/L, consistent with the negative

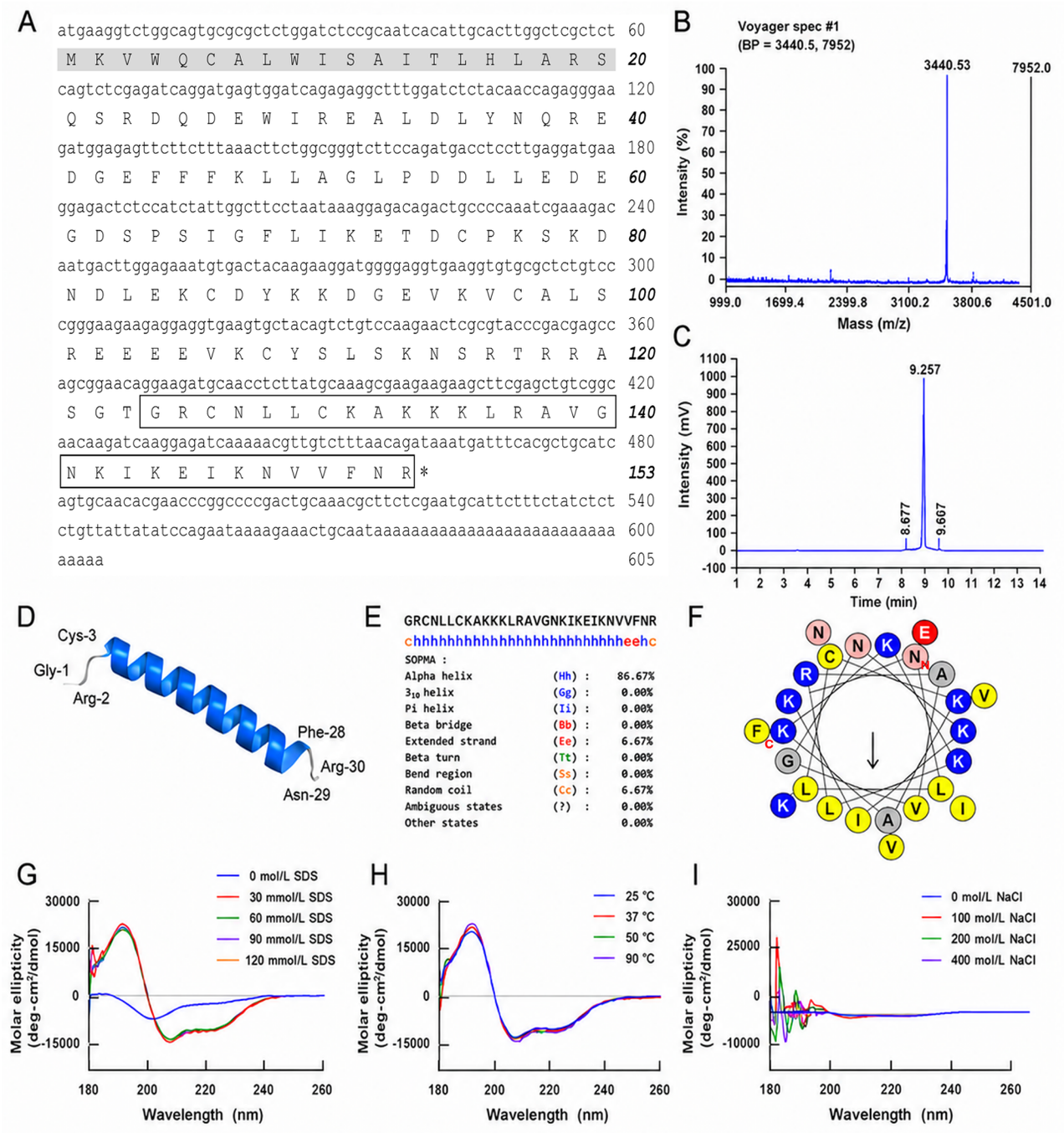

Figure 1 Sequence and structural characterization of HR-CATH2

A: cDNA and predicted precursor sequences of HR-CATH2. Gray background represents signal peptide region. Boxed part represents mature peptide sequence, with stop codon denoted with *. B: MALDI-TOF-MS identification of HR-CATH2 with disulfide bonds. C: RP-HPLC determination of HR-CATH2. D: Secondary structure of HR-CATH2 was predicted and visualized using PEP-FOLD3 and PyMOL, respectively. E: Secondary structure of HR-CATH2 predicted by SOPMA. F: Helix-wheel of HR-CATH2 plotted using the ExPASy proteomics server. Hydrophobic residues are displayed in gray and yellow, and hydrophilic residues are displayed in purple and blue. G: CD spectra of 50 μmol/L HR-CATH2 dissolved in different concentrations of SDS solution. H: CD spectra of 50 μmol/L HR-CATH2 dissolved in 60 mmol/L SDS at 25, 37, 50, and 90°C for 1 h. I: CD spectra of 50 μmol/L HR-CATH2 in solutions containing 60 mmol/L SDS plus indicated concentrations of NaCl.

control (Supplementary Table S2). Similarly, CCK-8 assays showed that HR-CATH2 at concentrations as high as 40 μmol/L did not impair the proliferation of A549 cells, HL-60 cells, RAW264.7 cells, or mouse splenocytes (Supplementary Figure S3).

LPS neutralization by HR-CATH2

As shown in Figure 2E and Supplementary Table S3, ITC demonstrated an exothermic interaction between HR-CATH2 and LPS, as indicated by the downward trend of the titration curve and the associated enthalpy changes. The dissociation constant (Kd) for binding to LPS was approximately 11.9 μmol/L. Binding reached saturation at 16 min, with an HR-CATH2:LPS molar ratio of 2.0. Consistent with these findings, SPRi showed progressively intensified signals when increasing concentrations of LPS were applied to HR-CATH2 immobilized on the chip (Figure 2F).

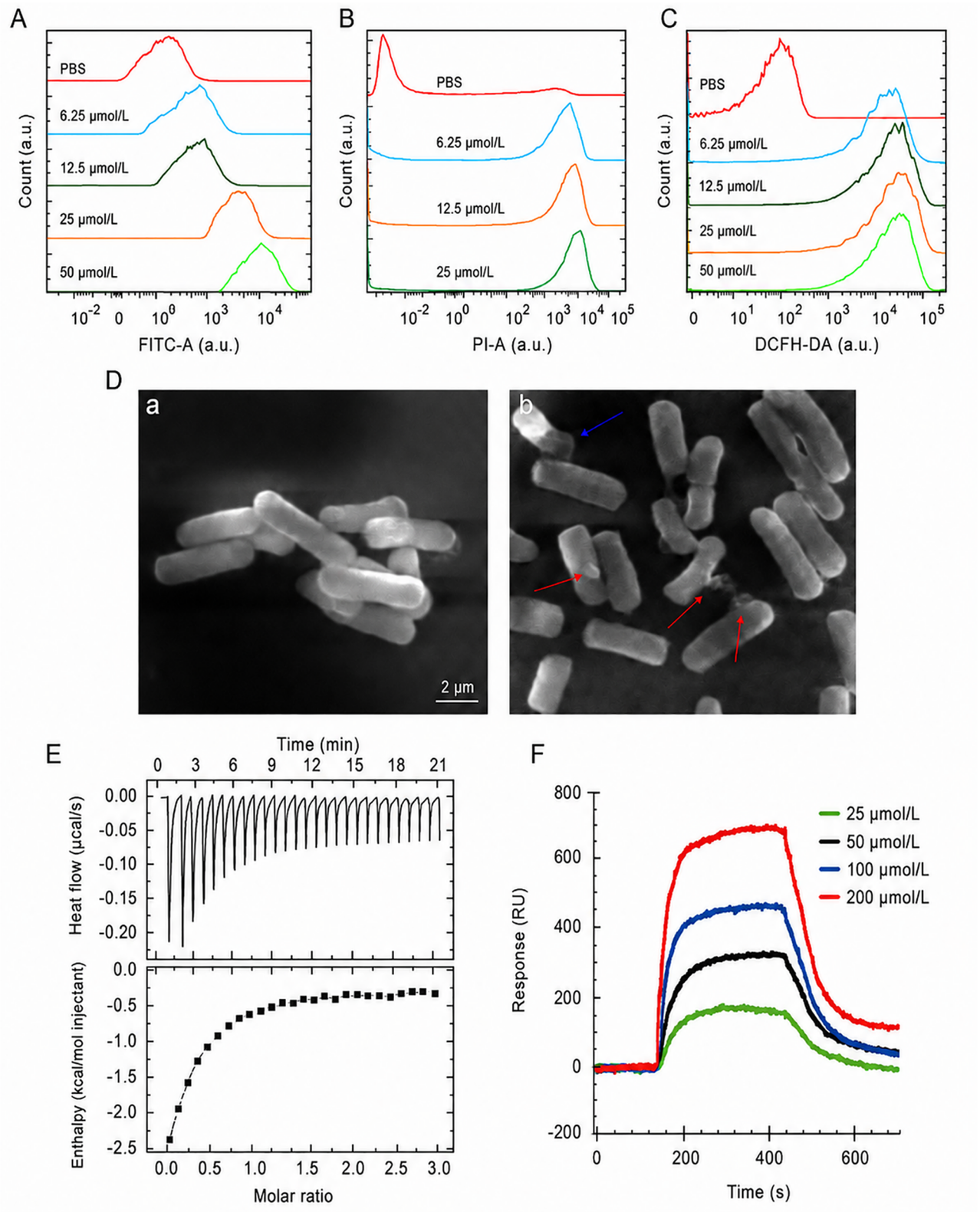

Figure 2 Antimicrobial mechanism of HR-CATH2 and its binding interaction with LPS

A–C: Flow cytometry analysis of *E. coli* ATCC 25922 after incubation with FITC-labeled HR-CATH2 (A), HR-CATH2+PI (B), and HR-CATH2+DCFH-DA (C). D: SEM images of *E. coli* ATCC 25922 after 45 min of treatment with PBS (a) or HR-CATH2 (2× MICs) (b). Membrane depressions are indicated by blue arrows, and membrane protrusions and structural damage are indicated by red arrows. E: ITC analysis of the interaction between HR-CATH2 and LPS. Upper panels show calorimetric changes during each titration as a function of time. Lower panels show integrated enthalpy changes plotted against the molar ratio of ligand to target (solid squares), with data fitted to a single-site binding model using MicroCal Origin (solid line). F: SPRi sensorgrams showing association and dissociation phases when LPS (25, 50, 100, and 200 μmol/L) was flowed over a gold chip with immobilized HR-CATH2.

Suppression of LPS-induced ROS production, proinflammatory factor expression, and inflammatory signaling pathway activation

As shown in Figure 3, LPS (100 ng/mL) markedly increased mRNA expression of inducible NO synthase (iNOS), IL-1β, TNF-*α*, and IL-6 in RAW264.7 cells and also increased expression of the corresponding proteins. HR-CATH2 attenuated these LPS-driven responses in a concentration-dependent manner. Specifically, HR-CATH2 suppressed LPS-induced transcription of iNOS, IL-1β, TNF-α, and IL-6 by approximately 31.0%–41.6%, 65.9%–99.4%, 57.9%–97.7%, and 69.5%–90.0%, respectively (Figure 3A–D). Suppression at the protein level was generally less pronounced than that observed at the mRNA level, with inhibition rates of approximately 0.6%–15.2%, 14.5%–90.9%, 81.9%–86.8%, and 16.1%–50.4%, respectively (Figure 3E–H). As excessive ROS generation can intensify oxidative stress and amplify inflammatory injury, intracellular ROS levels were evaluated with the fluorescent dye DCFH-DA. As shown in Figure 3I, LPS stimulation significantly increased ROS accumulation in RAW264.7 cells compared to untreated controls. Of note, HR-CATH2 markedly attenuated this LPS-induced ROS increase

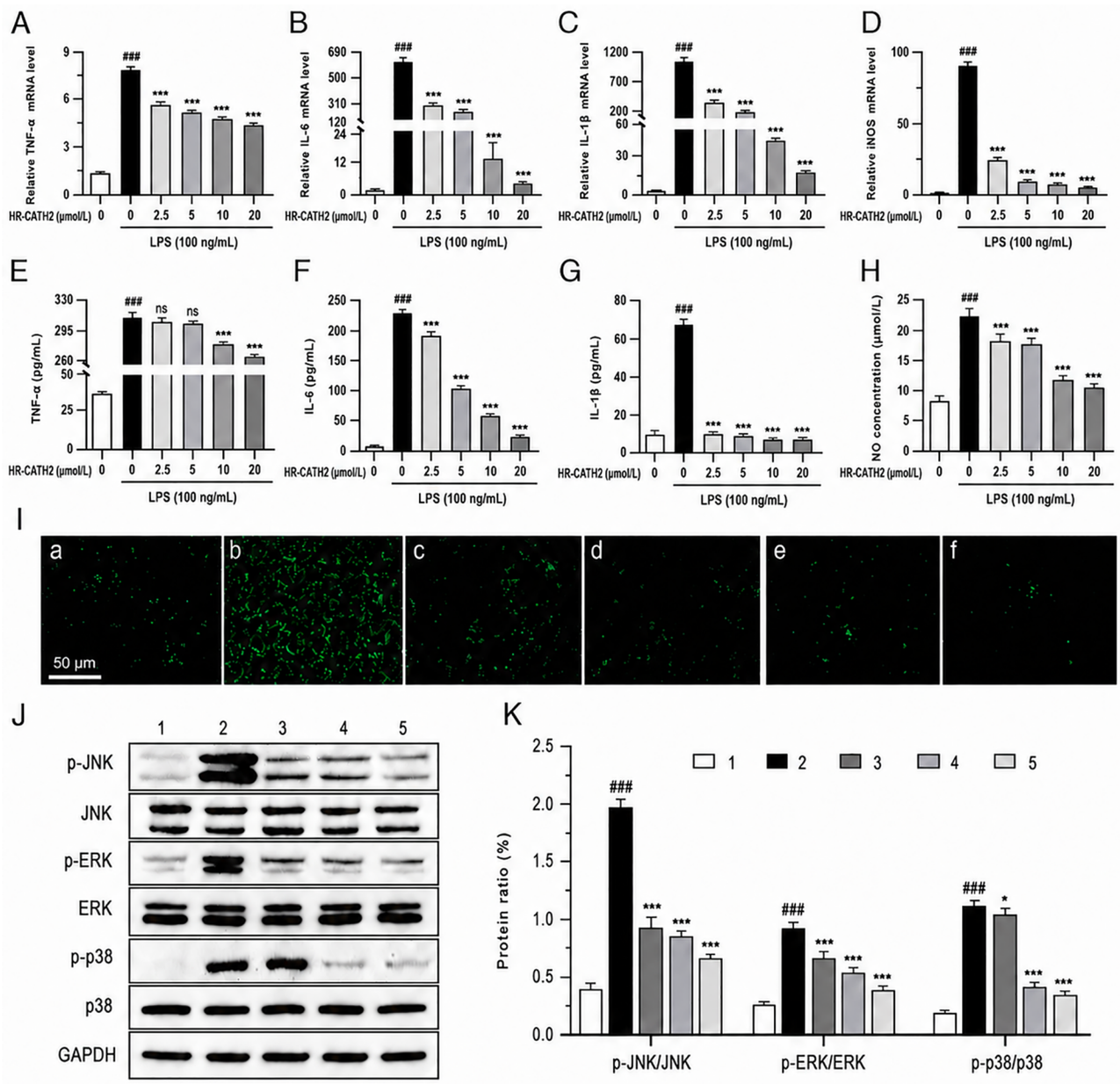

Figure 3 Effects of HR-CATH2 on LPS-induced ROS accumulation, nitrite production, and cytokine expression in RAW264.7 cells and activation of MAPK inflammatory signaling

A–D: mRNA expression of TNF-α (A), IL-6 (B), IL-1β (C), and iNOS (D). E–H: Production of TNF-α (E), IL-6 (F), IL-1β (G), and nitrite (H). I: Representative fluorescence images of RAW264.7 macrophages stained with DCFH-DA. Panels a–f correspond to cells treated with PBS, LPS (100 ng/mL), or LPS in combination with 2.5, 5, 10, and 20 μmol/L HR-CATH2, respectively. Images were obtained using a fluorescent inverted microscope at 100× magnification, Scale bar: 50 μm. J: Representative western blot images of p38, ERK, and JNK phosphorylation. K: Quantitative analysis of grayscale values of bands in panel J. ImageJ was used to analyze band density. Lines 1–5 correspond to cells incubated with PBS alone, LPS (100 ng/mL) alone, or LPS (100 ng/mL) in combination with HR-CATH2 at 2.5, 5, or 10 μmol/L. Data are presented as mean±SD (*n*=3). ###: *P*<0.001 versus control group; *: *P*<0.05 and ***: *P*<0.001 versus LPS-treated group; ns, not significant.

in a concentration-dependent manner.

To define the signaling basis underlying suppression of inflammatory mediator release, LPS-responsive MAPK activation was further examined. LPS exposure markedly increased phosphorylation of ERK, JNK, and p38 in RAW264.7 cells, whereas HR-CATH2 reduced this phosphorylation in a concentration-dependent manner without altering total ERK, JNK, or p38 protein levels (Figure 3J–K).

Direct anti-inflammatory activities of HR-CATH2 in macrophages

To investigate the direct anti-inflammatory activity of HR-CATH2 in macrophages, binding and intracellular localization of FITC-labeled HR-CATH2 in RAW264.7 cells were first examined by flow cytometry and fluorescence microscopy. As illustrated in Figure 4A, HR-CATH2 bound to RAW264.7 cells in a concentration-dependent manner, as reflected by the progressive increase in FITC fluorescence. Fluorescence microscopy further showed that FITC-labeled HR-CATH2 was detected within the DiI-labeled plasma membrane and was observed in proximity to, and partially overlapping with, the DAPI-stained nuclear region within 0.5 h, indicating cellular internalization and distribution within both cytoplasmic and nuclear compartments (Figure 4B). To determine whether HR-CATH2 exerted anti-inflammatory activity independent of LPS neutralization in macrophages, RAW264.7 cells were pretreated with HR-CATH2 for different durations before LPS stimulation. As demonstrated in Figure 4C, extension of the pretreatment period progressively strengthened the inhibitory effect of HR-CATH2 on LPS-induced IL-6 release. Notably, IL-6 production was significantly lower when macrophages were pretreated with HR-CATH2 for 2 h and washed before LPS exposure than under the reverse treatment sequence. Importantly, HR-CATH2 still reduced IL-6 accumulation by 48.86% even when administered after LPS stimulation (Figure 4D). Overall, these results suggest that HR-CATH2 may exert direct anti-inflammatory effects in macrophages through mechanisms not solely attributable to LPS neutralization.

To further define the molecular basis of this activity, transcriptomic profiling was performed in HR-CATH2-treated RAW264.7 cells. Compared with the control group, 114 genes were up-regulated and 26 genes were down-regulated following treatment (Figure 4E). Furthermore, GO analysis showed that the differentially expressed genes (DEGs) were predominantly enriched in pathways associated with MAPK kinase tyrosine/threonine phosphatase activity, inflammatory response, cellular response to LPS, TNF-α, IL-1, neutrophil chemotaxis, and negative regulation of NF-κB (Figure 4F). KEGG analysis further showed enrichment of DEGs in

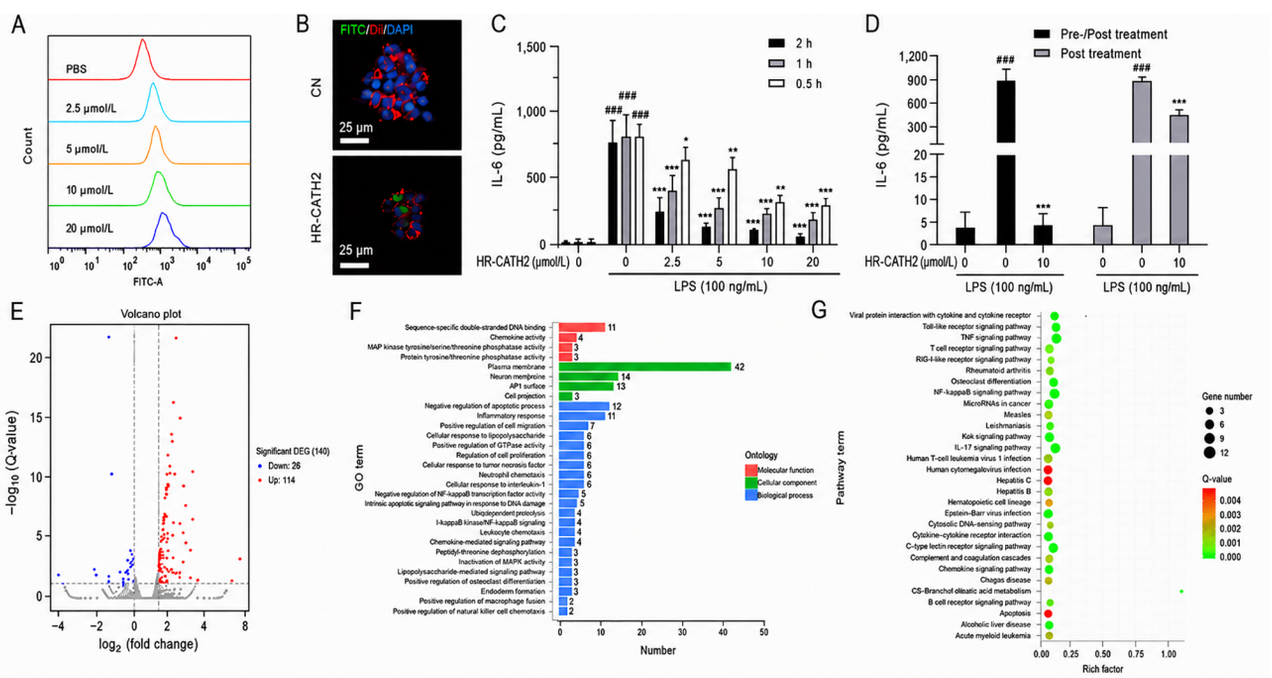

Figure 4 Direct anti-inflammatory effects of HR-CATH2 in macrophages

A: Flow cytometry analysis of FITC-labeled HR-CATH2 binding to RAW264.7 cells. B: Fluorescence microscopy images showing uptake of FITC-labeled HR-CATH2 by RAW264.7 cells. Cell membrane and nuclei were stained with DiI (red) and DAPI (blue), respectively. Scale bar: 25 μm. C: Effect of different pretreatment durations on suppression of IL-6 production by HR-CATH2 in LPS-stimulated RAW264.7 cells. RAW264.7 cells were preincubated with HR-CATH2 for 0.5, 1, and 2 h, washed thoroughly to remove unbound peptide, and then incubated with LPS for another 24 h before IL-6 measurement. D: Effect of different treatment regimens on suppression of IL-6 production by HR-CATH2 in LPS-stimulated RAW264.7 cells. For pretreatment, cells were incubated with HR-CATH2 at 20 μmol/L for 2 h, washed to remove unbound peptide, and incubated with LPS for another 24 h. For post-treatment, cells were treated with LPS for 2 h, washed to remove unbound LPS, and treated with HR-CATH2 at 20 μmol/L for another 24 h. $^{###}$: P<0.001 versus control group. *: P<0.05, ** P<0.01, and ***: P<0.001 versus LPS-treated group. E: Volcano plot of annotated transcriptome genes in RAW246.7 cells after exposure to 20 μmol/L HR-CATH2. The x-axis and y-axis represent fold change and statistical significance, respectively. Significant DEG thresholds were set to P<0.05 and |$\log_2$fold change|≥1. F: GO enrichment bar plot of DEGs in HR-CATH2-treated RAW264.7 cells. The x-axis represents the number of DEGs assigned to each term, and the y-axis represents enriched GO terms. G: KEGG enrichment scatter plot of DEGs in HR-CATH2-treated RAW264.7 cells. The x-axis represents the rich factor, dot size reflects the number of DEGs within each pathway, and dot color represents the range of Q values. Genes were classified according to functional relevance, and enriched pathways were selected based on the number of significant genes.

signaling pathways related to IL-17, Toll-like receptor, chemokine, NF-κB, and TNF signaling (Figure 4G). These findings further support the conclusion that HR-CATH2 directly targets inflammation-associated pathways and regulates macrophage function to produce anti-inflammatory effects.

Alleviation of CLP-induced sepsis by HR-CATH2

Given the combined antimicrobial, anti-inflammatory, and LPS-neutralizing activities of HR-CATH2, its therapeutic efficacy was evaluated in mice with CLP-induced sepsis. As displayed in Figure 5A, intraperitoneal injection of DXM (10 mg/kg) or HR-CATH2 (5 mg/kg) markedly improved survival at 72 h after CLP. Both treatments also alleviated clinical manifestations and reduced clinical scores at 24 h after CLP (Figure 5B). Consistent with these findings, blood leukocyte counts were markedly reduced in the CLP model group compared with the sham-operated group, whereas HR-CATH2 treatment effectively restored leukocyte levels (Figure 5C). In parallel, MPO activity and concentrations of IL-1β, TNF-*α*, MCP-1, and IL-6 were significantly elevated in serum and lung tissue from septic mice compared with the sham-operated controls, and these increases were significantly attenuated by both DXM and HR-CATH2 treatment (Figure 5D–L).

Histopathological analysis further supported the protective effect of HR-CATH2. Relative to the sham-operated group, hematoxylin and eosin (H&E) staining of tissues from the CLP model group revealed pronounced inflammatory cell infiltration, hemorrhage, pulmonary edema, and alveolar wall thickening in the lungs; hemorrhage, inflammatory cell infiltration, and disruption of normal hepatic plate architecture in the liver; and inflammatory cell infiltration, interstitial edema, and detachment of renal tubular epithelial cells in the kidney. In contrast, intraperitoneal injection of DXM or HR-CATH2 at 1 h after CLP significantly alleviated tissue injury induced by sepsis in these organs (Figure 5M–P).

DISCUSSION

The continued emergence and rapid global dissemination of antibiotic-resistant bacteria pose a major challenge to public health (Larsson & Flach, 2022; Willyard, 2017). In this context, AMPs have attracted substantial interest as alternatives to conventional anti-infective agents due to their low molecular weight, broad antimicrobial activity, distinct mechanisms of action, and comparatively low tendency to drive resistance (Lazzaro et al., 2020; Magana et al., 2020). Beyond direct microbicidal activity, AMPs also exert anti-inflammatory (Li et al., 2022; Xiao et al., 2022), antioxidant (Chai et al., 2022), anticancer (Deslouches & Di, 2017), and antiviral effects (Yu et al., 2021). In the present study, a previously unreported cathelicidin, HR-CATH2, was identified from the skin of *H. rugulosus*. This peptide displayed antimicrobial, LPS-neutralizing, and anti-inflammatory activities *in vitro* and alleviated sepsis in mice subjected to CLP. To the best of our knowledge, this peptide represents the first AMP derived from *H. rugulosus* with anti-sepsis activity.

AMPs commonly interact with membrane lipid bilayers and induce pore formation through mechanisms such as barrel-stave, carpet, and toroidal-pore models (Zhang et al., 2021), thereby destabilizing membrane integrity and ultimately causing cell death. Consistent with this general paradigm, HR-CATH2 showed clear bacterial membrane-binding activity, accompanied by marked disruption of *E. coli* membrane structure. In addition, HR-CATH2 markedly increased intracellular ROS production in *E. coli*, a response also reported for several other cathelicidins (Choi et al., 2017; Rowe-Magnus et al., 2019). These findings suggest that bactericidal activity of HR-CATH2 may involve both physical membrane damage and oxidative stress. However, the molecular basis by which HR-CATH2 promotes ROS accumulation in *E. coli* remains to be clarified.

Antimicrobial potency of AMPs is shaped by multiple structural determinants, particularly amino acid composition, amphiphilicity, and net positive charge (Huang et al., 2010; Xu & Lai, 2015). Similar to many frog-derived cathelicidins, HR-CATH2 adopted a typical amphipathic α-helical conformation and exhibited broad-spectrum antimicrobial activity. Of particular interest, some antifungal AMPs contain a conserved GXC(X3–9)C γ-core motif at the N-terminal region, in which X represents any amino acid. This motif forms a positively charged structural element that contributes to membrane disruption (Yount & Yeaman, 2004) and is closely associated with protein-membrane interactions (Utesch et al., 2018). HR-CATH2 also contained this motif in its primary sequence and showed antifungal activity against *Candida albicans*, with a MIC of 12.5 μmol/L. However, antifungal potency remained weaker than that reported for Cathelicidin-PP, another frog-derived cathelicidin containing a γ-core motif (Mu et al., 2017), despite almost identical amino acid composition within this region, with only lysine replacing arginine in Cathelicidin-PP. In addition, several cathelicidins lacking a γ-core motif, including Cathelicidin-PY (Wei et al., 2013), Cathelicidin-MH (Chai et al., 2021), and Cathelicidin-RC1 (Ling et al., 2014), also display antifungal activity against *C. albicans.* Together, these observations indicate that the γ-core motif alone is unlikely to determine antifungal capacity and suggest that residues outside this region may also make important contributions. Further investigation is required to define the structural basis underlying antifungal activity in HR-CATH2 and related AMPs.

TLR4, which is widely expressed in mouse macrophages, is activated by LPS and subsequently triggers MAPK signaling, production of multiple proinflammatory cytokines (Holani et al., 2020; Kong & Ge, 2008), and ROS accumulation (Shekhova, 2020; West et al., 2011). These responses are essential for pathogen clearance and host defense (Dryden, 2018; Shekhova, 2020). However, excessive cytokine release and ROS generation can drive uncontrolled inflammation and oxidative stress, ultimately leading to cellular injury and organ dysfunction (Lowes et al., 2013). In the present study, HR-CATH2 markedly suppressed LPS-induced production of proinflammatory cytokines and ROS and inhibited activation of the MAPK pathway in RAW264.7 cells. Given that HR-CATH2 can bind LPS, it is reasonable to assume that part of this inhibitory effect is attributable to LPS neutralization. Nevertheless, several cathelicidins, including CAP37-derived peptides, LL-37, CATH-2, and Hc-CATH, have also been shown to suppress the MAPK pathway and inflammatory mediator expression via interaction with macrophage surface receptors such as TLR4, followed by down-regulation of downstream signaling (Coorens et al., 2017; Schromm et al., 2021; Wei et al., 2013, 2015). Similarly, the present results showed that HR-CATH2 bound to macrophages and suppressed IL-6 production even in the absence of LPS, indicating an additional anti-inflammatory mechanism beyond LPS neutralization. Although available evidence did not support TLR4 as the relevant receptor for HR-CATH2 (Supplementary Figures S4, S5), transcriptomic analysis of HR-CATH2-treated RAW264.7 cells identified voltage-

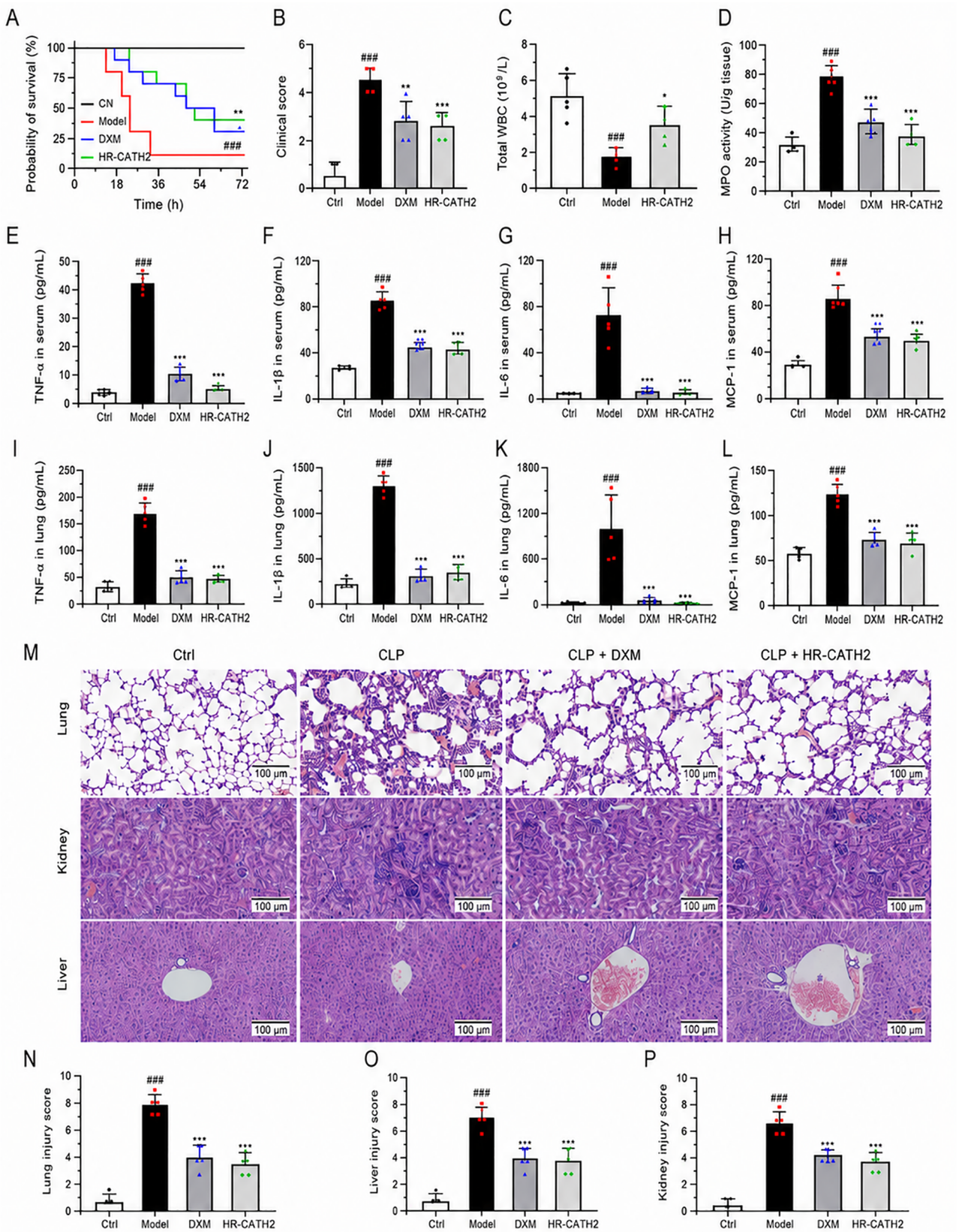

Figure 5 Effects of HR-CATH2 on CLP-induced sepsis in mice

A: Survival over 72 h. B: Clinical scores at 24 h. C: Blood leukocyte counts. D: MPO activity in lung tissues. E–L: Protein levels of MCP-1, TNF-α, IL-1β, and IL-6 in serum and lung tissues. M–P: Hematoxylin and eosin-stained sections of lung, kidney, and liver, together with corresponding injury scores. Scale bar: 100 μm. *n*=5. Ctrl: control, DXM: dexamethasone. ###: $P<0.001$ versus control group. *: $P<0.05$, **: $P<0.01$, and ***: $P<0.001$ versus CLP model group.

dependent anion channel 2 (VDAC2) as a potential binding partner. Definitive identification of the specific HR-CATH2 receptor will require further investigation, including pull-down assays coupled with mass spectrometry and direct binding analyses.

CLP can induce polymicrobial peritoneal infection that progresses to sepsis and death, and the inflammatory phenotype in CLP-induced septic mice closely resembles that observed in patients with sepsis (Rittirsch et al., 2009). Consistent with its *in vitro* activity, HR-CATH2 treatment improved survival in CLP-induced septic mice and ameliorated acute inflammatory injury in serum and major organs. Notably, relative to other cathelicidins with antimicrobial, LPS-neutralizing, and anti-inflammatory properties, including Cathelicidin-HG, Cathelicidin-MH, and FM-CATH, HR-CATH2 appeared to confer stronger therapeutic benefit in the CLP model at the same dose, potentially attributable to its direct anti-inflammatory effects mediated through receptor targeting in macrophages (Chai et al., 2021; Rittirsch et al., 2009; Wu et al., 2021; Xiong et al., 2024). Although early inflammatory activation of neutrophils and macrophages can facilitate pathogen clearance during the initial stage of sepsis, sustained or excessive activation can become deleterious during the intermediate and later stages, exacerbating organ damage and disease progression (He et al., 2023; Retter et al., 2025). Unlike cathelicidins such as Gy-CATH, OH-CATH30, CATHPb1, and PopuCATH, which enhance trafficking of macrophages, monocytes, and neutrophils to sites of infection and augment inflammatory responses, thereby potentially favoring efficacy during early sepsis, HR-CATH2 combines antimicrobial, LPS-neutralizing, and anti-inflammatory activities and may therefore provide benefit across multiple stages of disease (Cai et al., 2018; He et al., 2024; Li et al., 2013b; Yang et al., 2022).

HR-CATH2 contains only 30 amino acids, fewer than many peptides in the same family, a feature that may favor lower synthesis costs. In addition, HR-CATH2 showed high stability under elevated temperature and salt conditions together with low cytotoxicity. Collectively, these properties suggest that HR-CATH2 may be a promising candidate molecule for the development of therapeutics against bacterial inflammatory diseases, particularly sepsis, for which effective treatment remains limited. Furthermore, *H. rugulosus* has long been used in traditional Chinese medicine for relief of swelling and cough (Li et al., 2013a). Identification of HR-CATH2 therefore provides a plausible molecular basis for this traditional application and offers insight into defense strategies that may contribute to the survival of this frog species.

CONCLUSION

In summary, this study identified HR-CATH2 as a novel and highly stable cathelicidin from *H. rugulosus* with potent antimicrobial, anti-inflammatory and anti-sepsis activities. Notably, HR-CATH2 exerted rapid and effective antimicrobial activity through binding to bacterial cells, disrupting membrane integrity, and promoting oxidative stress. In addition, HR-CATH2 bound LPS and suppressed excessive production of proinflammatory cytokines and ROS in LPS-stimulated RAW264.7 cells. In the CLP-induced mouse model of sepsis, HR-CATH2 demonstrated clear therapeutic efficacy. To the best of our knowledge, HR-CATH2 represents the first cathelicidin derived from *H. rugulosus* reported to combine antimicrobial, LPS-neutralizing, and anti-inflammatory and anti-sepsis activities, highlighting its promise as a candidate molecule for the development of therapeutics against bacterial inflammatory diseases, particularly sepsis.

DATA AVAILABILITY

The raw transcriptome data have been deposited in NCBI (BioProject: PRJNA1470919), GSA (accession: CRA034383), and Science Data Bank (DOI: 10.57760/sciencedb. j00139.00325) via the ZR community portal.

SUPPLEMENTARY DATA

Supplementary data to this article can be found online.

COMPETING INTERESTS

The authors declare that they have no competing interests.

AUTHORS' CONTRIBUTIONS

H.L., S.L., and K.W. carried out the experiments, analyzed the data, and wrote the manuscript. J.C., W.Z., J.L., J.W., Y.L., and L.S. completed partial experiments, analyzed the data, and reviewed the manuscript. X.C. and Y.G. analyzed the data and reviewed the manuscript. X.X. conceived the project, designed the experiments, and wrote the manuscript. All authors read and approved the final version of the manuscript.

REFERENCES

Anders S, Huber W. 2010. Differential expression analysis for sequence count data. *Genome Biology*, **11**(10): R106.

Anders S, Pyl PT, Huber W. 2015. HTSeq—a Python framework to work with high-throughput sequencing data. *Bioinformatics*, **31**(2): 166–169.

Bals R, Wilson JM. 2003. Cathelicidins-a family of multifunctional antimicrobial peptides. *Cellular and Molecular Life Sciences CMLS*, **60**(4): 711–720.

Buchman AL. 2001. Side effects of corticosteroid therapy. *Journal of Clinical Gastroenterology*, **33**(4): 289–294.

Cai SS, Qiao X, Feng L, et al. 2018. Python cathelicidin CATHPb1 protects against multidrug-resistant staphylococcal infections by antimicrobial-immunomodulatory duality. *Journal of Medicinal Chemistry*, **61**(5): 2075–2086.

Cecconi M, Evans L, Levy M, et al. 2018. Sepsis and septic shock. *The Lancet*, **392**(10141): 75–87.

Chai JW, Chen X, Ye TF, et al. 2021. Characterization and functional analysis of Cathelicidin-MH, a novel frog-derived peptide with anti-septicemic properties. *eLife*, **10**: e64411.

Chai JW, Liu JF, Tian ML, et al. 2022. Multiple mechanistic action of brevinin-1FL peptide against oxidative stress effects in an acute inflammatory model of carrageenan-induced damage. *Oxidative Medicine and Cellular Longevity*, **2022**: 2615178.

Chai JW, Wu JN, Yang JX, et al. 2024. Cath-HG improves the survival rates and symptoms in LPS-induced septic mice due to its multifunctional properties. *International Immunopharmacology*, **143**(Pt 1): 113332.

Chen J, Lin YF, Chen JH, et al. 2021. Molecular characterization of cathelicidin in tiger frog (*Hoplobatrachus rugulosus*): antimicrobial activity and immunomodulatory activity. *Comparative Biochemistry and Physiology Part C: Toxicology & Pharmacology*, **247**: 109072.

Choi H, Yang ZL, Weisshaar JC. 2017. Oxidative stress induced in *E. coli* by the human antimicrobial peptide LL-37. *PLoS Pathogens*, **13**(6): e1006481.

Coorens M, Scheenstra MR, Veldhuizen EJA, et al. 2017. Interspecies cathelicidin comparison reveals divergence in antimicrobial activity, TLR modulation, chemokine induction and regulation of phagocytosis. *Scientific Reports*, **7**(1): 40874.

Curren EJ, Lutgring JD, Kabbani S, et al. 2022. Advancing diagnostic stewardship for healthcare-associated infections, antibiotic resistance, and sepsis. *Clinical Infectious Diseases*, **74**(4): 723–728.

Dawulieti J, Sun MD, Zhao YW, et al. 2020. Treatment of severe sepsis with nanoparticulate cell-free DNA scavengers. *Science Advances*, **6**(22): eaay7148.

Deslouches B, Di YP. 2017. Antimicrobial peptides with selective antitumor mechanisms: prospect for anticancer applications. *Oncotarget*, **8**(28): 46635–46651.

Dryden M. 2018. Reactive oxygen species: a novel antimicrobial. *International Journal of Antimicrobial Agents*, **51**(3): 299–303.

Fei L, Ye CY, Jiang JP. 2012. Colored Atlas of Chinese Amphibians and Their Distributions. Huayu Nature Book Trade Co. Ltd. (in Chinese)

He JW, Zhao S, Duan ML. 2023. The response of macrophages in sepsis-induced acute kidney injury. *Journal of Clinical Medicine*, **12**(3): 1101.

He YM, Ruan SM, Liang GZ, et al. 2024. A nonbactericidal anionic antimicrobial peptide provides prophylactic and therapeutic efficacies against bacterial infections in mice by immunomodulatory-antithrombotic duality. *Journal of Medicinal Chemistry*, **67**(9): 7487–7503.

Ho J, Chan H, Liang YH, et al. 2020. Cathelicidin preserves intestinal barrier function in polymicrobial sepsis. *Critical Care*, **24**(1): 47.

Holani R, Babbar A, Blyth GAD, et al. 2020. Cathelicidin-mediated lipopolysaccharide signaling via intracellular TLR4 in colonic epithelial cells evokes CXCL8 production. *Gut Microbes*, **12**(1): 1785802.

Huang YB, Huang JF, Chen YX. 2010. Alpha-helical cationic antimicrobial peptides: relationships of structure and function. *Protein & Cell*, **1**(2): 143–152.

Kanehisa M, Furumichi M, Tanabe M, et al. 2017. KEGG: New perspectives on genomes, pathways, diseases and drugs. *Nucleic Acids Research*, **45**(D1): D353–D361.

Kim D, Paggi JM, Park C, et al. 2019. Graph-based genome alignment and genotyping with HISAT2 and HISAT-genotype. *Nature Biotechnology*, **37**(8): 907–915.

Kong L, Ge BX. 2008. MyD88-independent activation of a novel actin-Cdc42/Rac pathway is required for Toll-like receptor-stimulated phagocytosis. *Cell Research*, **18**(7): 745–755.

Kościuczuk EM, Lisowski P, Jarczak J, et al. 2012. Cathelicidins: family of antimicrobial peptides. A review. *Molecular Biology Reports*, **39**(12): 10957–10970.

Larsson DGJ, Flach CF. 2022. Antibiotic resistance in the environment. *Nature Reviews Microbiology*, **20**(5): 257–269.

Lazzaro BP, Zasloff M, Rolff J. 2020. Antimicrobial peptides: application informed by evolution. *Science*, **368**(6490): eaau5480.

Li H, Handsaker B, Wysoker A, et al. 2009. The Sequence Alignment/Map format and SAMtools. *Bioinformatics*, **25**(16): 2078–2079.

Li J, Chordia MD, Zhang Y, et al. 2022. Critical role of FPR1 in splenocyte migration into brain to worsen inflammation and ischemic brain injury in mice. *Theranostics*, **12**(7): 3024–3044.

Li J, Huang LQ, Qu XB. 2013a. Medicinal Fauna of China. 2nd ed. Fuzhou: Fujian Science and Technology Press. (in Chinese)

Li SA, Xiang Y, Wang YJ, et al. 2013b. Naturally occurring antimicrobial peptide OH-CATH30 selectively regulates the innate immune response to protect against sepsis. *Journal of Medicinal Chemistry*, **56**(22): 9136–9145.

Li Z, Song YQ, Yuan PS, et al. 2020. Antibacterial fusion protein BPI21/LL-37 modification enhances the therapeutic efficacy of hUC-MSCs in sepsis. *Molecular Therapy*, **28**(8): 1806–1817.

Ling GY, Gao JX, Zhang SM, et al. 2014. Cathelicidins from the bullfrog *Rana catesbeiana* provides novel template for peptide antibiotic design. *PLoS One*, **9**(3): e93216.

Liu VX, Fielding-Singh V, Greene JD, et al. 2017. The timing of early antibiotics and hospital mortality in sepsis. *American Journal of Respiratory and Critical Care Medicine*, **196**(7): 856–863.

Lowes DA, Webster NR, Murphy MP, et al. 2013. Antioxidants that protect mitochondria reduce interleukin-6 and oxidative stress, improve mitochondrial function, and reduce biochemical markers of organ dysfunction in a rat model of acute sepsis. *British Journal of Anaesthesia*, **110**(3): 472–480.

Magana M, Pushpanathan M, Santos AL, et al. 2020. The value of antimicrobial peptides in the age of resistance. *The Lancet Infectious Diseases*, **20**(9): e216–e230.

Mu LX, Zhou L, Yang JJ, et al. 2017. The first identified cathelicidin from tree frogs possesses anti-inflammatory and partial LPS neutralization activities. *Amino Acids*, **49**(9): 1571–1585.

Martin M. 2011. Cutadapt removes adapter sequences from high-throughput sequencing reads. *EMBnet. journal*, **17**(1): 10–12.

Pantic JM, Mechkarska M, Lukic ML, et al. 2014. Effects of tigerinin peptides on cytokine production by mouse peritoneal macrophages and spleen cells and by human peripheral blood mononuclear cells. *Biochimie*, **101**: 83–92.

Retter A, Singer M, Annane D. 2025. "The NET effect": neutrophil extracellular traps-a potential key component of the dysregulated host immune response in sepsis. *Critical Care*, **29**(1): 59.

Rhodes A, Evans LE, Alhazzani W, et al. 2017. Surviving sepsis campaign: international guidelines for management of sepsis and septic shock: 2016. *Intensive Care Medicine*, **43**(3): 304–377.

Rittirsch D, Huber-Lang MS, Flierl MA, et al. 2009. Immunodesign of experimental sepsis by cecal ligation and puncture. *Nature Protocols*, **4**(1): 31–36.

Rowe-Magnus DA, Kao AY, Prieto AC, et al. 2019. Cathelicidin peptides restrict bacterial growth via membrane perturbation and induction of reactive oxygen species. *mBio*, **10**(5): e02021–19.

Schromm AB, Paulowski L, Kaconis Y, et al. 2021. Cathelicidin and PMB neutralize endotoxins by multifactorial mechanisms including LPS interaction and targeting of host cell membranes. *Proceedings of the National Academy of Sciences of the United States of America*, **118**(27): e2101721118.

Shekhova E. 2020. Mitochondrial reactive oxygen species as major effectors of antimicrobial immunity. *PLoS Pathogens*, **16**(5): e1008470.

Shen S, Park JW, Lu ZX, et al. 2014. rMATS: Robust and flexible detection of differential alternative splicing from replicate RNA-Seq data. *Proceedings of the National Academy of Sciences of the United States of America*, **111**(51): E5593–E5601.

Tian ML, Liu JF, Chai JW, et al. 2021. Antimicrobial and anti-inflammatory effects of a novel peptide from the skin of frog *Microhyla pulchra*. *Frontiers in Pharmacology*, **12**: 783108.

Tian ML, Wang K, Liang Y, et al. 2023. The first Brevinin-1 antimicrobial peptide with LPS-neutralizing and anti-inflammatory activities *in vitro* and *in vivo*. *Frontiers in Microbiology*, **14**: 1102576.

Utesch T, de Miguel Catalina A, Schattenberg C, et al. 2018. A computational modeling approach predicts interaction of the antifungal protein AFP from *Aspergillus giganteus* with fungal membranes via its γ-core motif. *mSphere*, **3**(5): e00377–18.

Vandewalle J, Timmermans S, Paakinaho V, et al. 2021. Combined glucocorticoid resistance and hyperlactatemia contributes to lethal shock in sepsis. *Cell Metabolism*, **33**(9): 1763–1776. e5.

Wang K, Li M, Hakonarson H. 2010. ANNOVAR: Functional annotation of genetic variants from high-throughput sequencing data. *Nucleic Acids Research*, **38**(16): e164.

Wang L, Wang SQ, Li W. 2012. RSeQC: quality control of RNA-seq experiments. *Bioinformatics*, **28**(16): 2184–2185.

Wang T, Cui YZ, Jin JJ, et al. 2013. Translating mRNAs strongly correlate to proteins in a multivariate manner and their translation ratios are phenotype specific. *Nucleic Acids Research*, **41**(9): 4743–4754.

Wei L, Gao JX, Zhang SM, et al. 2015. Identification and characterization of the first cathelicidin from sea snakes with potent antimicrobial and anti-inflammatory activity and special mechanism. *Journal of Biological Chemistry*, **290**(27): 16633–16652.

Wei L, Yang JJ, He XQ, et al. 2013. Structure and function of a potent lipopolysaccharide-binding antimicrobial and anti-inflammatory peptide. *Journal of Medicinal Chemistry*, **56**(9): 3546–3556.

West AP, Brodsky IE, Rahner C, et al. 2011. TLR signalling augments macrophage bactericidal activity through mitochondrial ROS. *Nature*, **472**(7344): 476–480.

Willyard C. 2017. The drug-resistant bacteria that pose the greatest health threats. *Nature*, **543**(7643): 15.

Wiriyaampaiwong P, Karnmongkol C, Punpad A, et al. 2022. Cathelicidin-HR from *Hoplobatrachus rugulosus*: an antioxidant peptide that performs a protective effect against UV/H_2O_2 -induced DNA damage. *Journal of Applied Biology & Biotechnology*, **10**(4): 35–44.

Wong JH, Ye XJ, Ng TB. 2013. Cathelicidins: peptides with antimicrobial, immunomodulatory, anti-inflammatory, angiogenic, anticancer and procancer activities. *Current Protein & Peptide Science*, **14**(6): 504–514.

Wu JN, Xiong WC, Li JQ, et al. 2023. Peptide TK-HR from the skin of Chinese folk medicine frog *Hoplobatrachus Rugulosus* accelerates wound healing via the activation of the neurokinin-1 receptor. *Journal of Medicinal Chemistry*, **66**(23): 16002–16017.

Wu JN, Zhang HY, Chen XX, et al. 2021. FM-CATH, a novel cathelicidin from *Fejervarya Multistriata*, shows therapeutic potential for treatment of CLP-induced sepsis. *Frontiers in Pharmacology*, **12**: 731056.

Xiao X, Lu H, Zhu WT, et al. 2022. A novel antimicrobial peptide derived from bony fish IFN1 exerts potent antimicrobial and anti-inflammatory activity in mammals. *Microbiology Spectrum*, **10**(2): e02013–21.

Xiong WC, Chai JW, Wu JN, et al. 2024. Cathelicidin-HG alleviates sepsis-induced platelet dysfunction by inhibiting GPVI-mediated platelet activation. *Research*, **7**: 0381.

Xu XQ, Lai R. 2015. The chemistry and biological activities of peptides from amphibian skin secretions. *Chemical Reviews*, **115**(4): 1760–1846.

Yang Y, Wu J, Li Q, et al. 2022. A non-bactericidal cathelicidin provides prophylactic efficacy against bacterial infection by driving phagocyte influx. *eLife*, **11**: e72849.

Ye ZF, Fu L, Li SY, et al. 2024. Synergistic collaboration between AMPs and non-direct antimicrobial cationic peptides. *Nature Communications*, **15**(1): 7319.

Young MD, Wakefield MJ, Smyth GK, et al. 2010. Gene ontology analysis for RNA-seq: accounting for selection bias. *Genome Biology*, **11**(1): R14.

Yount NY, Yeaman MR. 2004. Multidimensional signatures in antimicrobial peptides. *Proceedings of the National Academy of Sciences of the United States of America*, **101**(19): 7363–7368.

Yu J, Dai Y, Fu YX, et al. 2021. Cathelicidin antimicrobial peptides suppress EV71 infection via regulating antiviral response and inhibiting viral binding. *Antiviral Research*, **187**: 105021.

Zanetti M, Gennaro R, Scocchi M, et al. 2002. Structure and biology of cathelicidins. *In*: Keisari Y, Ofek I. The Biology and Pathology of Innate Immunity Mechanisms. New York: Springer, 203–218.

Zeng BS, Chai JW, Deng ZH, et al. 2018. Functional characterization of a novel lipopolysaccharide-binding antimicrobial and anti-Inflammatory peptide in vitro and in vivo. *Journal of Medicinal Chemistry*, **61**(23): 10709–10723.

Zhang QY, Yan ZB, Meng YM, et al. 2021. Antimicrobial peptides: mechanism of action, activity and clinical potential. *Military Medical Research*, **8**(1): 48.